Applied Thermal Engineering 48 (2012) 495–505

Contents lists available at SciVerse ScienceDirect

Applied Thermal Engineering

journal homepage: www.elsevier.com/locate/apthermeng

A framework for the optimization of integrated energy systems

Neera Jain*, Andrew G. Alleyne

University of Illinois at Urbana-Champaign, 158 MEB, M/C 244, 1206 W. Green St., Urbana, IL 61801, USA

HIGHLIGHTS

- We introduce an exergy-based framework for steady-state optimization and control of integrated energy systems.
- Exergy destruction describes irreversibilities across multiple energy domains making it an apt efficiency metric for IESs.
- Minimization of the objective function generates feedforward (FF) control input signal to achieve optimal setpoints.
- Robustness of the control signals to model uncertainty is demonstrated through a case study using validated system models.
- The physical significance of an exergy-based objective function makes it easily generalizable to complex IESs.

ARTICLE INFO

Article history:
Received 24 May 2011
Accepted 2 April 2012
Available online 3 May 2012

Keywords:
Optimization
Control
Exergy analysis
Integrated energy systems

ABSTRACT

This paper introduces an exergy-based objective function for the steady-state optimization and control of integrated energy systems (IESs). The use of exergy destruction as the metric for minimization enables the objective function to be scalable with respect to (1) subsystem configuration and (2) subsystem capacity, thereby rendering the approach generalizable to a wide class of IESs. More specifically, exergy destruction can be used to characterize irreversibilities across multiple energy domains (chemical, electrical, mechanical, thermal) which makes it very suitable for the types of energy subsystems which comprise IESs. The approach presented in this paper couples the exergy-based optimization with a feedforward control framework which uses static models to estimate the control inputs required to achieve the optimal setpoints. It is shown that the physical significance obtained using an objective function derived from first-principles makes the objective modular and therefore easily generalizable to complex IESs.

© 2012 Elsevier Ltd. All rights reserved.

1. Introduction and motivation

Integrated energy systems (IESs) combine prime-mover technologies, such as internal combustion (IC) engines, and/or fuel cells, with other technologies which directly utilize the power produced by the prime-mover and/or utilize the thermal energy otherwise wasted in the production of power. IESs can be thought of as complex systems comprised of many interconnected heterogenous subsystems such as the prime-movers listed above, thermally-activated heating systems, desiccant dehumidifiers, vapor-compression refrigeration systems, and/or energy storage systems [1]. A key feature of the IES heterogeneity is that it typically spans multiple energy domains – chemical, electrical, mechanical, and thermal – as evidenced by the examples of subsystems which comprise IESs.

IESs are becoming more prevalent because of their environmental, reliability, economic, and efficiency benefits [1–3]. Many researchers have conducted thermodynamic analyses of IESs to optimize design parameters and production costs in these systems. Specifically, exergy-based analysis has been widely used to evaluate and optimize IESs at the design stage because of its ability to accurately capture the effect of irreversibilities and produce results which respect the physical limitations imposed by both the first and second laws of thermodynamics [4–7]. However, to fully realize the benefits of IESs, effective control of these systems is required. Through online optimization and control, systems can effectively respond to disturbances such as weather or varying loads that cannot be accounted for at the design stage [8–12].

The critical component of any optimization problem is the definition of the objective function. A common minimization metric for IESs is operational cost (in dollars) [12–15]; however, this metric does not explicitly consider the efficiency of the IES which is heavily dependent on the level of irreversibility in the system (which in turn also has environmental implications). Moreover, economic metrics do not accurately capture the underlying physics which govern the behavior of the system, particularly because these metrics are typically empirically-derived. In [9], the

* Corresponding author. Tel.: +1 217 244 6556.
E-mail addresses: njain2@illinois.edu (N. Jain), alleyne@illinois.edu (A.G. Alleyne).

1359-4311/$ – see front matter © 2012 Elsevier Ltd. All rights reserved.
doi:10.1016/j.applthermaleng.2012.04.003

Nomenclature

α	heat transfer coefficient
a	aperture
A	area
C	cooling capacity
δ	displacement
E	energy
F	fraction of coil surface covered by fins
θ	angle
h	specific enthalpy
k	coeff. of conductivity
K	flow coefficient
$\dot{m}$	mass flow rate
η	efficiency
p	percent of total power
P	pressure
$\dot{Q}$	heat transfer rate
ρ	density
s	specific entropy
S	entropy
T	temperature
u	specific internal energy
u	vector of control inputs
UA	overall heat transfer coefficient
v	vector of optimization variables
V	volume
$\dot{W}$	work transfer rate
ω	rotational speed
X	exergy

Subscript

0	reference (dead) state
1–4	VCC transition points
$1'$–$4'$	Otto cycle transition points
a	air
adb	adiabatic
AF	air–fuel mixture
c	condenser
dest	destroyed
e	evaporator
eng	engine
f	fan
gen	generated
H	high-temperature reservoir
i	interior
k	compressor
L	low-temperature reservoir
o	outer
r	refrigerant
sat	saturated
sys	system
tp	throttle plate
v	electronic expansion valve
vol	volumetric

authors advocate the consideration of different minimization metrics, but the proposed objective functions for energy and CO_2 emissions are empirically-based modifications of an objective function again based on electricity and fuel costs. [8] proposes an objective function which also minimizes the daily operation cost of a micro combined heat and power (μCHP) system but is generalizable for various systems within the class of μCHP systems. However, the optimization variables are only the electrical and thermal inputs/outputs of various subsystems such as the input to a thermal storage device; the operation of the thermal storage device itself is not optimized with respect to the amount of heat it must store.

What is lacking among these examples is an objective function with the following 3 key properties:

1. Generalizability with respect to overall IES subsystem configuration,
2. Scalability with respect to system capacity,
3. Control-oriented.

The focus of this paper is the design of a physics-based objective function for the optimization of IES operation which embodies these 3 properties.

1. Scalability with architecture

IESs are often comprised of a diversity of subsystems arranged in different architectures or configurations [1,8]. Therefore, we seek an objective function which is modular so that it can be revised appropriately for different systems in a systematic way.

A major challenge in designing a modular objective function comes from the fact that the individual subsystems which comprise IESs are heterogenous and typically characterized using different efficiency metrics. For example, IC engines are often characterized in terms of their fuel efficiency whereas heat and cooling systems are typically characterized in terms coefficient of performance (COP). It is difficult to combine these metrics in a meaningful way that preserves the physics of the system.

This paper addresses this challenge by evaluating the operation setpoints and control inputs needed to minimize the total exergy destruction throughout the system while satisfying specified performance criteria and constraints. The exergy destruction minimization objective will be constructed as the sum of the exergy destruction in each subsystem of the IES. This will provide a common and modular metric for evaluating the efficiency of the complete system since exergy can be used to characterize irreversibilities across multiple energy domains (chemical, electrical, mechanical, thermal). The use of exergy is also motivated by its widespread use for the analysis and design of IESs cited earlier [4–7].

2. Scalability with size

In addition to diversity with respect to architecture, IESs are designed across a large range of capacities (to produce power, cooling, etc.) [1]. Consider a diesel engine. The model parameters for a small diesel engine will necessarily be different than those for a much larger horsepower engine, but the dynamics of both systems will be governed by the Diesel cycle. This is a feature of most energy systems. Therefore, the objective function design will be based on thermodynamic cycles which describe the behavior of the various energy subsystems rather than on specific component design parameters.

3. Control-oriented

Our goal is to optimize system behavior during operation. Therefore the optimization and control framework must be

designed so that the system setpoints and control inputs can be optimized online. The approach presented here will be to couple the exergy-based objective function with a feedforward control framework which uses nonlinear static models to estimate the control inputs required to achieve the optimal setpoints (Fig. 1).

In the following sections, we present a framework for developing a generalizable, control-oriented, exergy-based objective function. The objective function will be developed for an engine-driven vapor-compression (refrigeration) cycle (VCC) system depicted schematically in Fig. 2. These systems are used in a variety of applications and at different scales; common examples include (in order of increasing size) automotive air-conditioning systems, transport refrigeration systems [16], and engine-driven chillers [1]. Nevertheless, the dynamics of spark-ignited IC engines and vapor-compression systems are governed by the Otto cycle and vapor-compression cycle (VCC), respectively, in all of these applications. Therefore, the exergy-based approach will be effective in developing an optimization and control framework that satisfies the three criteria discussed earlier.

This paper is organized as follows. The vapor-compression cycle (VCC), Otto cycle, and the concept of exergy, are briefly reviewed in Sec. 2. In Sec. 3, the main development of the exergy-based objective function is presented. In Sec. 4, static model equations are used to define design constraints for the optimization problem, and a case study is presented which compares the exergy-based objective function to subsystem-specific efficiency metrics. The feedforward control framework is presented in Sec. 5 along with a robustness analysis to model uncertainty and assumptions. Finally, conclusions of this work are summarized in Sec. 6.

2. Background

2.1. Thermodynamic cycles

In this paper we consider a VCC system driven by a spark-ignited internal combustion (SI–IC) engine. The thermodynamic cycles governing the behavior of these two-subsystems are the vapor-compression cycle (VCC) and the Otto cycle, respectively.

2.1.1. Vapor-compression cycle

The standard VCC consists of four processes of the refrigerant: compression (1–2), condensation (2–3), expansion (3–4), and evaporation (4–1), where 1, 2, 3, and 4 refer to the transition points of the cycle pictured on a pressure-enthalpy (P–h) diagram shown in Fig. 3(a). The VCC assumes the following:

i. Isobaric condensation and evaporation
ii. Isenthalpic expansion
iii. Isentropic compression
iv. Evaporation of refrigerant to a saturated or superheated vapor state, and
v Condensation of refrigerant to a saturated or subcooled liquid state.

Based on the constitutive relationships between pressure, temperature, entropy, etc. [17], the VCC has four thermodynamic degrees of freedom (DOFs). The three specific enthalpies of the cycle, $\{h_1, h_2, h_3 = h_4\}$, and any one of the following three quantities,

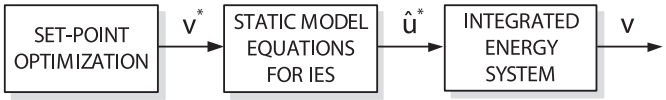

Fig. 1. Schematic of optimization and feedforward control framework.

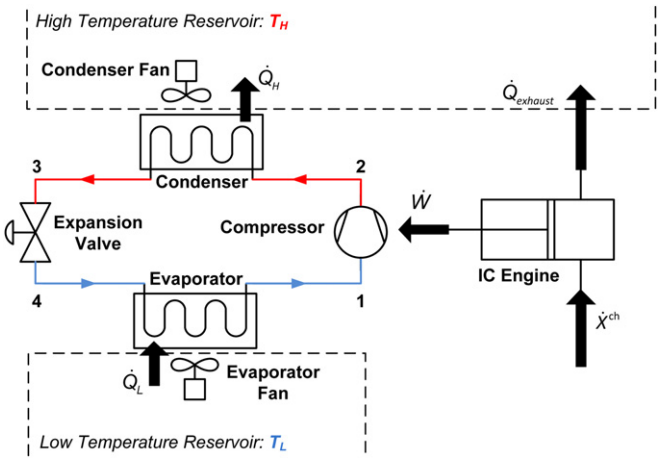

Fig. 2. Schematic of engine-driven VCC system.

$\{P_1, P_2, \text{or } T_1\}$, uniquely define the remaining thermodynamic states at each of the transition points given the assumptions outlined above. However, to actually compute critical quantities of interest, such as the amount of cooling that is achieved Equation (1), or the amount of power consumed Equation (2), there is an additional DOF which must be considered: the refrigerant mass flow rate, $\dot{m}_r$. This DOF is a fluid dynamic variable, rather than a thermodynamic variable, and is not captured in the P–h diagram of the VCC.

$$\dot{Q}_L = \dot{m}_r(h_1 - h_4) \tag{1}$$

$$\dot{W}_{\text{VCC}} = \dot{m}_r(h_2 - h_1) \tag{2}$$

2.1.2. Otto cycle

The Otto cycle describes the dynamics of a spark-ignited internal combustion (SI–IC) engine. We do not consider the intake stroke and instead begin the analysis at point 1′ in Fig. 3(b) where we assume that the working fluid is a stoichiometric air–fuel mixture (i.e. the equivalence ratio, φ, equals 1) [18]. We also model the exhaust stroke as heat rejection to the ambient environment. Therefore, we can characterize the Otto cycle as the sequence of four processes of the air–fuel mixture: compression ($1'$–$2'$), combustion ($2'$–$3'$), expansion ($3'$–$4'$), and heat rejection ($4'$–$1'$), where $1'$, $2'$, $3'$, and $4'$ refer to the transition points of the cycle pictured on a pressure–volume (P–V) diagram shown in Fig. 3(b). The ideal Otto cycle assumes the following:

i. Isentropic compression
ii. Isochoric and adiabatic combustion
iii. Isentropic expansion
iv. Isochoric heat rejection

In addition to the assumptions outlined above, we assume that the combustion reaction is stoichiometric, and that the combustion reactants and products are gaseous and form ideal gas mixtures. Therefore, once $T_{1'}, P_{1'}$, and $r = V_{1'}/V_{2'}$ (the compression ratio of the engine) are specified, the thermodynamic properties at each of the states in the Otto cycle are determined [18]. The only optimization variable is the mass flow rate of the air–fuel mixture, $\dot{m}_{\text{AF}}$. (Note that in turbo-charged SI–IC engines, $P_{1'}$ is a DOF that can be optimized.)

2.2. Exergy

The first law of thermodynamics is a statement of energy conservation. The second law introduces the notion of entropy

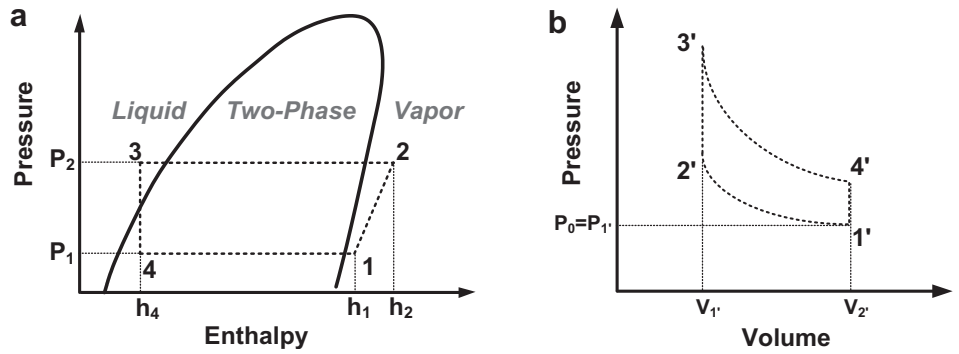

Fig. 3. (a) P–h diagram of the standard vapor-compression cycle, (b) P–V diagram of the ideal Otto cycle.

and connects it to the irreversibility that is observed in natural phenomena by postulating that a process can only proceed in "the direction that causes the total entropy of the system plus surroundings to increase" [17]. It is the combination of the first and second laws of thermodynamics that is particularly powerful. Exergy (also referred to as "availability") is defined as the maximum reversible work that can be extracted from a substance at a given state during its interaction with a given environment.

Whereas energy is always conserved, exergy is not. Similarly to energy, exergy can be transferred in three ways: by heat transfer, work, or through mass exchange with the environment. However, contrary to energy, exergy is destroyed during irreversible phenomena such as chemical reaction, mixing, and viscous dissipation. The amount of exergy destroyed in a system or through a process is a measure of the loss of potential to do work.

Equation (3) is the total exergy balance for a closed system, i.e., a system that does not exchange mass with its surroundings. Therefore, it contains terms characterizing the rate at which exergy is transferred only by heat transfer and work transfer. The quantities T_0 and P_0 are the temperature and pressure, respectively, of the reference environment. The reference environment is typically chosen as an infinite reservoir with which the system is interacting, such as the ambient environment. The use of a reference environment for defining exergy is consistent with the way in which all forms of potential energy are defined.

$$\underbrace{\sum_j \left(1-\frac{T_0}{T_j}\right)\dot{Q}_j}_{\substack{\text{rate of exergy transfer}\\ \text{accompanying heat transfer}}} - \underbrace{\left(\dot{W}-P_0\frac{dV_{sys}}{dt}\right)}_{\substack{\text{rate of exergy transfer}\\ \text{accompanying work transfer}}} - \underbrace{T_0\dot{S}_{gen}}_{\substack{\text{rate of exergy}\\ \text{destruction}}} + \underbrace{\dot{X}^{\text{ch}}}_{\substack{\text{rate at which}\\ \text{chemical exergy is}\\ \text{added to system}}} = \underbrace{\frac{dX_{sys}}{dt}}_{\substack{\text{total rate of}\\ \text{exergy transfer}}} \tag{3}$$

A feature of exergy is that in addition to characterizing thermal and mechanical potential, it can also characterize chemical potential. This is represented by the term $\dot{X}^{\text{ch}}$ in Equation (3), the rate at which chemical exergy is added to the system. For example, in the case of combustion, the chemical exergy is the maximum reversible work that can be extracted through the reaction of the fuel with environmental components [17].

3. Objective function development

Integrated energy systems (IESs) are characterized by two primary objectives: 1) meet specified performance demand, and 2) maximize system efficiency. It is necessary to define a mathematical function that captures these objectives for each subsystem of a given IES and can be minimized or maximized to yield an optimal solution.

We seek an objective function in which the exergy destruction in the overall system is minimized during operation. In general, this can be expressed in a modular additive form as

$$J = \lambda_1 J_{\text{subsystem},1} + \lambda_2 J_{\text{subsystem},2} + \cdots + \lambda_n J_{\text{subsystem},n} \tag{4}$$

where $J_{\text{subsystem},i}$ is the rate of exergy destruction in subsystem i, λ_i is a weighting factor on $J_{\text{subsystem},i}$, and J is the total rate of exergy destruction throughout the IES. In the following subsections we derive the objective function for an engine-driven VCC system, which can be expressed as

$$J = \lambda \cdot J_{\text{Otto}} + J_{\text{VCC}} \tag{5}$$

where J is the total objective function. We consider a single weighting factor, λ, for this two-subsystem case. Both J_{Otto} and J_{VCC} can be derived using the exergy balance for a closed system Equation (3). In the case of the VCC, only thermo-mechanical exergy exists. In the case of the Otto cycle, chemical exergy must also be accounted for.

3.1. Vapor-compression cycle

Since the VCC is closed and cyclic, we consider only exergy transferred by heat and work transfer and apply the exergy balance (without chemical exergy) in rate form as shown in Equation (6) where T_j is the boundary temperature at which the heat transfer $\dot{Q}_j$ occurs.

$$\underbrace{\sum_j \left(1-\frac{T_0}{T_j}\right)\dot{Q}_j}_{\substack{\text{rate of exergy transfer}\\ \text{accompanying heat transfer}}} - \underbrace{\left(\dot{W}-P_0\frac{\mathrm{d}V_{\text{sys}}}{\mathrm{d}t}\right)}_{\substack{\text{rate of exergy transfer}\\ \text{accompanying work}}} - \underbrace{T_0\dot{S}_{\text{gen}}}_{\substack{\text{rate of exergy}\\ \text{destruction}}} = \underbrace{\frac{\mathrm{d}X_{\text{sys}}}{dt}}_{\substack{\text{total rate of}\\ \text{exergy transfer}}} \tag{6}$$

During steady-state operation, Equation (6) reduces to

$$\dot{X}_{\text{dest,VCC}} = T_H \dot{S}_{\text{gen,VCC}} = -(-\dot{W}_{\text{VCC}}) + \left(1 - \frac{T_H}{T_L}\right)\dot{Q}_L \tag{7}$$

where T_0 has been replaced by T_H and T_j has been replaced by T_L [19]. Equation (7) is evaluated with T_H and T_L in degrees Kelvin. Applying the first law of thermodynamics to the VCC yields

$$\dot{W}_{\text{VCC}} = \dot{Q}_H - \dot{Q}_L = \dot{m}_r(h_2 - h_3) - \dot{m}_r(h_1 - h_4). \tag{8}$$

Substituting Equation (8) into Equation (7) yields

$$J_{\text{VCC}} = \dot{X}_{\text{dest,VCC}} = \dot{m}_r(h_1 - h_4)\left(1 - \frac{T_H}{T_L}\right) + \dot{m}_r(h_2 - h_1) \geq 0 \tag{9}$$

which is solely a function of h_1, h_2, h_4, and $\dot{m}_r$; the assumption of isenthalpic expansion implies $h_3 = h_4$. By virtue of the physical nature of these thermodynamic variables, the following inequalities hold:

$$-1 < \left(1 - \frac{T_H}{T_L}\right) \leq 0 \tag{10}$$

$$\dot{m}_r(h_2 - h_1) > 0 \tag{11}$$

$$\dot{m}_r(h_1 - h_4) > 0. \tag{12}$$

If the cycle was operated without any losses due to irreversibility, or equivalently, $\dot{X}_{\text{dest,VCC}} = 0$, then the following equality must hold:

$$\left|\dot{m}_r(h_1 - h_4)\left(1 - \frac{T_H}{T_L}\right)\right| = \dot{m}_r(h_2 - h_1). \tag{13}$$

However, in reality,

$$\left|\dot{m}_r(h_1 - h_4)\left(1 - \frac{T_H}{T_L}\right)\right| < \dot{m}_r(h_2 - h_1). \tag{14}$$

Therefore, J_{VCC} is nonnegative and its theoretical minimum value is zero.

The minimization of J_{VCC} is subject to the following thermodynamic constraints:

i. $h_1 < h_2$,
ii. $h_4 < h_1$,
iii. $T_1 \leq T_L$,
iv. $T_3 \leq T_H$,
v. $T_1 - T_4 \geq 0$,
vi. $T_{3,\text{sat}} - T_3 \geq 0$

where $T_{3,\text{sat}}$ is the saturated temperature at P_2. The first two constraints ensure that compression and evaporation, respectively, occur. The third and fourth constraints impose the correct temperature gradients during evaporation and condensation, respectively. The fifth constraint ensures that only refrigerant vapor is compressed. Finally, the sixth constraint ensures that only refrigerant liquid is expanded. The performance constraint is given as

$$\left|\frac{C_{\text{desired}} - C_{\text{achieved}}}{C_{\text{desired}}}\right| \leq \gamma, \quad 0 \leq \gamma \leq 1 \tag{15}$$

where C_{desired} and γ are inputs to the optimization problem and $C_{\text{achieved}} = \dot{Q}_L = \dot{m}_r(h_1 - h_4)$. The parameter γ allows the user to relax the constraint on C_{desired} for applications in which a small deviation from the desired cooling capacity is allowable.

3.2. Otto cycle

We consider the Otto cycle as a closed system in which the control mass is the air–fuel mixture in the engine cylinder. For the Otto cycle, Equation (3) in non-rate form simplifies to

$$\begin{aligned} X_{\text{dest,Otto}} &= T_H S_{\text{gen,Otto}} = X^{\text{ch}} - W_{\text{net}} \\ &= X^{\text{ch}} - (W_{\text{expansion}} - W_{\text{compression}}) \end{aligned} \tag{16}$$

which can be further expanded as

$$X_{\text{dest,Otto}} = X^{\text{ch}} - ((u_{3'} - u_{4'}) - (u_{2'} - u_{1'})) \tag{17}$$

where u is specific internal energy, $1'$, $2'$, $3'$, and $4'$ refer to the transition points of the cycle shown in Fig. 3, and X^{ch} is equal to 5.413 kJ/mol for octane (C_8H_{18}) at the standard reference state. The value for X^{ch} varies with temperature, but the variation is sufficiently small that X^{ch} is often approximated as constant [17]. If a fuel other than octane is used, X^{ch} can be easily modified.

Equation (17) is the amount of exergy destroyed in a single Otto cycle per unit mass of air–fuel mixture. In order to express Equation (17) in units of power, we multiply Equation (17) by the mass flow rate of the air–fuel mixture.

$$J_{\text{Otto}} = \dot{X}_{\text{dest,Otto}} = \dot{m}_{\text{AF}}\left[X^{\text{ch}} - ((u_{3'} - u_{4'}) - (u_{2'} - u_{1'}))\right] \geq 0 \tag{18}$$

The minimization of J_{Otto} is subject to the following performance constraint:

$$\dot{W}_{\text{achieved}} = \dot{m}_{\text{AF}}(u_{3'} - u_{4'}) \geq \dot{W}_{\text{desired}}. \tag{19}$$

3.3. Complete objective function

The complete objective function is

$$\begin{aligned} J = {} & \lambda\left(\dot{m}_{\text{AF}}\left[X^{\text{ch}} - ((u_{3'} - u_{4'}) - (u_{2'} - u_{1'}))\right]\right) \\ & + \left(\dot{m}_r(h_1 - h_4)\left(1 - \frac{T_H}{T_L}\right) + \dot{m}_r(h_2 - h_1)\right) \end{aligned} \tag{20}$$

and the inputs to the optimization problem are:

i. Desired cooling capacity, C_{desired}
ii. Performance deviation tolerance, γ
iii. Weighting factor, λ
iv. Low-temperature reservoir temperature, T_L
v. High-temperature reservoir temperature, T_H
vi. Engine compression ratio, r
vii. Temperature of air–fuel mixture at transition point $1'$, $T_{1'}$
viii. Pressure of air–fuel mixture at transition point $1'$, $P_{1'}$
ix. Chemical exergy of fuel, X^{ch}

The complete vector of optimization variables is

$$\mathbf{v} = \begin{pmatrix} \mathbf{v}_{\text{VCC}} & \mathbf{v}_{\text{Otto}} \end{pmatrix}^T \in \Re^6 \tag{21}$$

where

$$\mathbf{v}_{\text{VCC}} = \begin{pmatrix} h_1 & h_2 & h_4 & P_1 & \dot{m}_r \end{pmatrix} \in \Re^5 \tag{22}$$

and

$$\mathbf{v}_{\text{Otto}} = \begin{pmatrix} \dot{m}_{\text{AF}} \end{pmatrix} \in \Re. \tag{23}$$

The solution to the optimization problem is

$$\mathbf{v}^* = \arg\min_{v}(J) = \begin{pmatrix} h_1^* & h_2^* & h_4^* & P_1^* & \dot{m}_r^* & \dot{m}_{AF}^* \end{pmatrix}^T \in \Re^6. \quad (24)$$

and is subject to the thermodynamic constraints described above. While J_{VCC} and J_{Otto} can be derived independently of one another, it is the solution of the coupled problem that is of interest. Specifically, the power required to achieve the desired cooling capacity in the VCC is the desired power input to the Otto cycle: $\dot{W}_{desired} = \dot{W}_{VCC} = \dot{m}_r(h_2 - h_1)$. At this point, we have only considered thermodynamic and fluid dynamic constraints. In the next section, we will define design constraints which must be considered in the optimization problem for this particular IES.

4. Case study

The objective function developed in the previous section was derived based on first-principles in order to maintain generalizability. However, the hardware in a particular IES constrains the performance and efficiency achievable by that system when it is operated. In this section, we define a set of design constraints to impose on the optimization problem. We will then present a case study which demonstrates the advantages of the exergy-based optimization over an optimization with respect to subsystem-specific efficiency metrics.

4.1. Design constraints

The design constraints developed here necessarily require some level of empiricism due to the performance maps and correlations which are widely used to model many thermodynamic systems. Nevertheless, in the framework proposed in this paper, empiricism is limited to the design constraints; the objective itself remains unchanged for different engine-driven VCC systems.

4.1.1. VCC system

The steady-state behavior of a standard VCC system is described by the following 9 equations:

$$\hat{K}_v = f_1(a_v, P_1, P_2) \quad (25)$$

$$\hat{\eta}_{vol,k} = f_2(\omega_k, P_1, P_2) \quad (26)$$

$$\hat{\dot{m}}_{r,v} = \hat{K}_v\sqrt{\rho_3(P_2 - P_1)} \quad (27)$$

$$\hat{\dot{m}}_{r,k} = \hat{\eta}_{vol,k}\delta_k\omega_k\rho_1 \quad (28)$$

$$\hat{\dot{m}}_{r,v} = \hat{\dot{m}}_{r,k} \quad (29)$$

$$\widehat{(UA)}_L = f_3\left(p_{f,e}, P_1, h_4, \dot{m}_r, \dot{m}_{a,e}\right) \quad (30)$$

$$\widehat{(UA)}_H = f_4\left(p_{f,c}, P_2, \dot{m}_r, \dot{m}_{a,c}\right) \quad (31)$$

$$\hat{\dot{Q}}_L = \widehat{(UA)}_L(T_L - T_4) = \dot{m}_r(h_1 - h_4) \quad (32)$$

$$\hat{\dot{Q}}_H = \widehat{(UA)}_H(T_3 - T_H) = \dot{m}_r(h_2 - h_4) \quad (33)$$

where $\hat{K}_v$ is the valve flow coefficient, $\hat{\eta}_{vol}$ is the compressor volumetric efficiency, and $\widehat{(UA)}_L$ and $\widehat{(UA)}_H$ are the overall heat transfer coefficients [20] at the low and high-temperature reservoirs, respectively. The functions f_1, f_2, f_3, and f_4 are empirically-derived nonlinear relationships provided in Appendix A for the particular VCC system which will be considered in the subsequent case study.

We define the vector of control inputs (described in Table 1) to the VCC system as

$$\mathbf{u}_{VCC} = \begin{pmatrix} a_v & \omega_k & p_{f,e} & p_{f,c} \end{pmatrix}. \quad (34)$$

Each component in the VCC system must be considered when defining the design constraints to be imposed on the optimization problem. First we consider the two heat exchangers (condenser and evaporator) as well as their corresponding fans. The design constraints imposed by these components are defined in Equations (35) and (36) where $(UA)_{L,max}$ and $(UA)_{H,max}$ are described in Appendix A.

$$\dot{Q}_{L,max} \geq \dot{Q}_L \Leftrightarrow (UA)_{L,max}(T_L - T_4) \geq \dot{m}_r(h_1 - h_4) \quad (35)$$

$$\dot{Q}_{H,max} \geq \dot{Q}_H \Leftrightarrow (UA)_{H,max}(T_3 - T_H) \geq \dot{m}_r(h_2 - h_4) \quad (36)$$

Next we consider the EEV and compressor. The design constraints imposed by these components, Equations (37) and (38) respectively, are expressed in terms of their individual control inputs. Equations (25)–(29) are solved at each iteration for a_v and ω_k to ensure that the values are feasible.

$$0\% < a_v \leq 100\% \quad (37)$$

$$0 \text{ rpm} < \omega_k \leq 1800 \text{ rpm} \quad (38)$$

4.1.2. Spark-ignited internal combustion (SI–IC) engine

The steady-state behavior of an SI–IC engine is described by the following equations:

$$\hat{\tau}_{friction} = \hat{b}_{eng}\omega_k \quad (39)$$

$$\hat{\tau}_{load} = \frac{\dot{W}_{VCC}}{\omega_k} \quad (40)$$

$$\hat{\tau}_{total} = \hat{\tau}_{friction} + \hat{\tau}_{load} \quad (41)$$

$$\hat{\dot{W}}_{desired,total} = \hat{\tau}_{total}\omega_k \quad (42)$$

$$\hat{\theta}_{tp} = f_5(\dot{m}_{AF}) \quad (43)$$

$$\hat{\eta}_{vol,eng} = f_6(\omega_k) \quad (44)$$

where $\hat{\tau}_{friction}$ is the torque applied to the engine due to friction ($\hat{b}_{eng}$ is an engine parameter) and $\hat{\tau}_{load}$ is the torque applied to the engine by virtue of the compressor in the VCC system. The input to the SI–IC engine is the throttle angle, θ_{tp}, which is a nonlinear function of $\dot{m}_{AF}$. The volumetric efficiency of the engine is described by f_6. The functions f_5 and f_6 are given in Appendix A for the specific

Table 1
VCC System control inputs.

Input	Description
a_v	Electronic expansion valve (EEV) aperture (percent open)
ω_k	Compressor speed (rpm)
$p_{f,e}$	Evaporator fan power (percent of maximum)
$p_{f,c}$	Condenser fan power (percent of maximum)

SI–IC engine model considered here. The design constraints imposed by the engine are

$$\dot{W}_{\text{achieved}} \geq \dot{W}_{\text{desired,total}}$$
$$\eta_{\text{vol,eng}}\dot{m}_{\text{AF}}(u_{3'} - u_{4'}) \geq \left(\tau_{\text{friction}} + \tau_{\text{load}}\right)\omega_k \quad (45)$$

and

$$13.3^{\circ} \leq \theta_{\text{tp}} \leq 80^{\circ}. \quad (46)$$

Equation (45) replaces the original performance constraint on the Otto cycle, Equation (19).

4.2. Case study

The optimization problem consists of the nonlinear objective function, J, as well as multiple nonlinear constraints, and is therefore solved using the function *fmincon* in the MATLAB Optimization Toolbox [21]. Details regarding the convergence of the solution are provided in Appendix B.

In this case study we compare the exergy-based objective function against an alternative objective function. The two cases are described below.

Case 1: The optimization of the IES with respect to the exergy-based objective function, J, which we will redefine as $J_{\text{Case 1}}$ below.

$$J_{\text{Case 1}} = J = \lambda \cdot J_{\text{Otto}} + J_{\text{VCC}} \quad (47)$$

Case 2: The optimization of the IES with respect to an efficiency objective in which standard efficiency metrics for each of the subsystems are added together. The VCC system is optimized with respect to the coefficient of performance (COP) [22] and the SI–IC engine is optimized with respect to the rate of fuel consumption [23–25]. A higher COP corresponds to more efficient performance, so in order to maximize COP, its inverse is minimized [26] as shown in Equation (48).

$$J_{\text{Case 2}} = \frac{1}{\text{COP}} + \dot{m}_{\text{fuel}} = \frac{h_2 - h_1}{h_1 - h_4} + \dot{m}_{\text{fuel}} \quad (48)$$

where

$$\dot{m}_{\text{fuel}} = \frac{\dot{m}_{\text{AF}}}{15.7} \quad (49)$$

by virtue of the following two relationships:

$$\dot{m}_{\text{AF}} = \dot{m}_{\text{fuel}} + \dot{m}_{\text{air}} \quad (50)$$

$$\frac{\dot{m}_{\text{air}}}{\dot{m}_{\text{fuel}}} = 14.7. \quad (51)$$

In each case, the optimization problem was solved for the same set of optimization variables with identical constraints and the following input parameters:

$$C_{\text{desired}} = 0.8 \text{ kW} \qquad T_L = 15^{\circ}\text{C}$$
$$\gamma = 0 \qquad r = 8$$
$$\lambda = 1 \qquad T_{1'} = T_H$$
$$T_H = 27^{\circ}\text{C} \qquad P_{1'} = 101.3 \text{ kPa}$$

Remark. $\gamma = 0$ indicates that the optimization was constrained to provide exactly the desired cooling capacity, C_{desired}.

The results are shown in Table 2. We make the following observations:

1. Both objective functions achieve very similar performance with respect to the VCC optimization variables.
2. In Case 2, the optimal value of $\dot{m}_{\text{AF}}$ is significantly higher than the optimal value achieved in Case 1.

Table 2
Comparison of Cases 1 and 2.

Optimization variable	Units	Case 1	Case 2
h_1	kJ/kg	257	257
h_2	kJ/kg	281	281
h_4	kJ/kg	104	105
P_1	kPa	288	288
$\dot{m}_r$	kg/hr	18.8	18.9
$\dot{m}_{\text{AF}}$	kg/hr	1.06	2.58
$J_{\text{Case 1}}$	kW	0.664	–
$J_{\text{Case 2}}$	N/A	–	0.156
C_{achieved}	kW	0.800	0.800

The primary disadvantage of $J_{\text{Case 2}}$ is its lack of physical significance due to its mixed dimensions. The rate of fuel consumption term in $J_{\text{Case 2}}$ is in units of kg/s whereas COP is dimensionless. When the objective function is not physics-based, as is the case for $J_{\text{Case 2}}$, the various terms may not be appropriately balanced, potentially resulting in an inefficient solution. This is highlighted in Case 2 where the optimal value of $\dot{m}_{\text{AF}}$ is very large compared to the optimal value achieved in Case 1.

From the derivation of $\dot{X}_{\text{dest,Otto}}$ in Sec. 3, we see that the rate of exergy destruction in the Otto cycle is directly proportional to $\dot{m}_{\text{AF}}$. Therefore the solution to the exergy-based optimization, Case 1, results in a significantly lower rate of exergy destruction than operating with the setpoints achieved in Case 2. This is due in large part to the fact that in the exergy-based objective function, J_{Otto} and J_{VCC} represent the same physical quantity, rate of exergy destruction. Consequently, their relative magnitudes are such that one term is not inappropriately weighted significantly more than the other.

For this two-subsystem IES, we can introduce a weighting coefficient into $J_{\text{Case 2}}$ Equation (52) so that the two efficiency terms are more equally weighted. The weighting coefficient, λ_2, was chosen to be 3600 which is equivalent to optimizing $\dot{m}_{\text{fuel}}$ in kg/hr rather than kg/s. The results are shown in Table 3.

$$J_{\text{Case 2}} = \frac{1}{\text{COP}} + \lambda_2 \cdot \dot{m}_{\text{fuel}} \quad (52)$$

As expected, the weighted Case 2 produces a more efficient solution than in the unweighted Case 2. Despite the improvement in efficiency, this highlights a fundamental flaw of $J_{\text{Case 2}}$, namely its sensitivity to weighting parameters that inherently must be heuristically chosen. More importantly, when summing different efficiency metrics, each potentially expressed in different units, choosing appropriate weighting coefficients will become increasingly difficult as the number of subsystems increases.

In contrast, exergy obeys the law of superposition so with each additional subsystem in a particular IES, the complete objective function, Equation (4), can be easily augmented with an additive

Table 3
Comparison of weighted and unweighted Case 2.

Optimization variable	Units	Case 2 with $\lambda_2 = 1$	Case 2 with $\lambda_2 = 3600$
h_1	kJ/kg	257	257
h_2	kJ/kg	281	281
h_4	kJ/kg	105	104
P_1	kPa	288	288
$\dot{m}_r$	kg/hr	18.9	18.9
$\dot{m}_{AF}$	kg/hr	2.58	1.09
C_{achieved}	kW	0.800	0.800

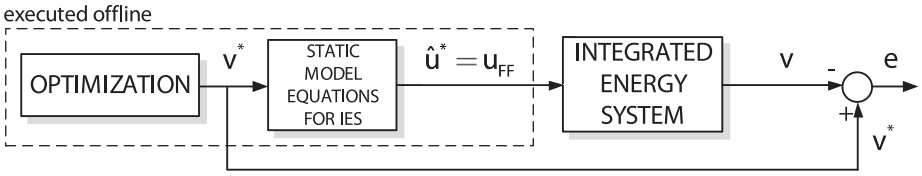

Fig. 4. Schematic describing optimization and feedforward control framework.

term representing the same quantity, rate of exergy destruction. This property is critical to satisfying our goal of developing a generalizable objective function for IESs.

5. Control and robustness

In order to operate a given system at its optimal setpoints, we propose a feedforward control framework in which the steady-state control inputs, $\hat{\mathbf{u}}^*$, are determined by solving the static model equations of the system. We will then demonstrate the robustness of this approach to model uncertainty in a simulation environment using a validated system model.

5.1. Feedforward control framework

Once $\mathbf{v}^*$ has been determined, $\hat{\mathbf{u}}^*$ can be determined by solving Equations (25)–(33) and (43). The hat notation is used to denote that $\hat{\mathbf{u}}^*$ is obtained based on the functions f_1–f_6 which have some associated uncertainty. For example, for f_1 the uncertainty is defined as

$$|K_v - \hat{K}_v| = \tilde{K}_v \geq 0. \tag{53}$$

The elements of $\hat{\mathbf{u}}^*$ are analogous to model-based feedforward control input signals (Fig. 4). Typically the model uncertainty is nonzero, and therefore,

$$|\mathbf{u}^* - \hat{\mathbf{u}}^*| = \tilde{\mathbf{u}} \geq 0. \tag{54}$$

and

$$|\mathbf{v}^* - \mathbf{v}| = \mathbf{e} \geq 0. \tag{55}$$

The robustness of $\mathbf{e}$ to $\tilde{\mathbf{u}}$ will be demonstrated in the next section.

5.2. Robustness to model uncertainty

Now we demonstrate the robustness of the optimization approach to modeling uncertainty and assumptions used to estimate the feedforward control inputs $\hat{\mathbf{u}}^* = \mathbf{u}_{\mathrm{FF}}$.

The feedforward control inputs needed to achieve the optimal setpoints generated by solving J in Sec. 4 are shown in Table 4. These input values were used in the system simulation model [27,28]. Eight perturbation cases were considered (Table 5). In each case, two different parameters were perturbed by either +10% or −10%, thereby introducing uncertainty into f_1–f_6. Additionally, there are three modeling assumptions which are made at the optimization and control stage which do not hold in the system model. As will be seen, results of the approach are suitably robust despite these simplifying assumptions:

1. *No pressure or heat losses between components in the VCC system.* The system simulation model contains pipe models which characterize pressure losses and heat transfer which occur as the refrigerant travels between components in the VCC system.
2. *The refrigerant in each heat exchanger is entirely a two-phase fluid.* The lumped-parameter moving boundary modeling approach [27] which is used to model each heat exchanger accurately captures the presence of multiple fluid regions if necessary and calculates the heat transfer through each region using the appropriate heat transfer coefficients.
3. *T_H and T_L are constant throughout the condenser and evaporator, respectively.* In each heat exchanger model, the lumped air temperature (for heat transfer calculations) is taken to be a weighted sum of the inlet and outlet air temperatures.

The validity of these assumptions affects the accuracy of f_3 Equation (30) and f_4 Equation (31) in each of the eight perturbation cases.

The comparison between the optimal setpoints and simulated setpoints for four of the optimization variables – h_1, h_2, h_4, and P_1 – is shown on a P–h diagram in Fig. 5 with more detailed views shown in Fig. 6 and Fig. 7. We can see that the variation is very small, and the average deviation of any one variable is within 6% of the optimal value (Table 6).

Table 4
Model-based feedforward control inputs.

Control input	Units	Value
a_v	%	10.5
$p_{f,e}$	%	58.0
$p_{f,c}$	%	83.4
θ_{tp}	deg	40.6

Table 5
Modeling uncertainty perturbation cases.

		$\eta_{\upsilon ol,eng}$, +10%	b_e, −10%
$\eta_{\upsilon ol,k}$, +10%	+10%	Case 1	Case 5
K_v, −10%	−10%	Case 2	Case 6
$\alpha_{r,e}$, +10%	+10%	Case 3	Case 7
$\alpha_{a,c}$, −10%	−10%	Case 4	Case 8

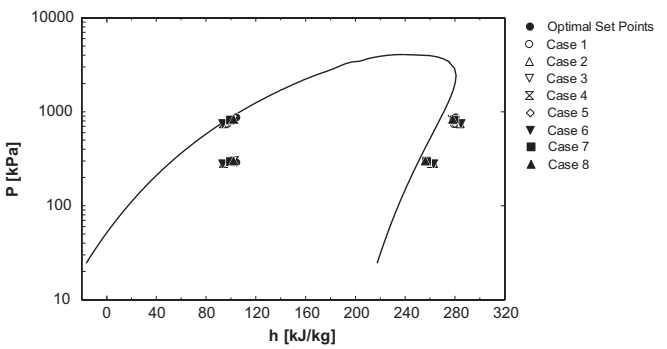

Fig. 5. P–h diagram comparing optimal setpoints for thermodynamic DOFs of the VCC system with the setpoints achieved in simulation under various cases of model uncertainty.

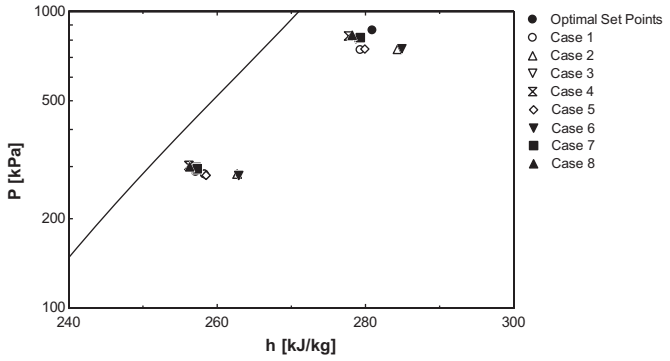

Fig. 6. Close up of VCC transition points 1 and 2 from Fig. 5.

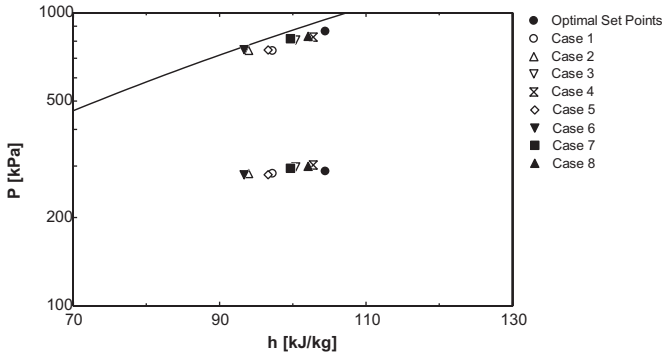

Fig. 7. Close up of VCC transition points 3 and 4 from Fig. 5.

The optimization variables $\dot{m}_r$ and $\dot{m}_{AF}$ cannot be depicted on a P–h diagram. Therefore, we evaluated the value of the objective function, J, as well as the achieved cooling capacity, $C_{achieved}$, for each of the eight cases and compared it to J^* (Fig. 8) and $C^*_{achieved}$, (Fig. 9) respectively. The values of J and $C_{achieved}$ in all eight cases were well within 10% of the optimal values, J^* and $C^*_{achieved}$, demonstrating the robustness of the feedforward control approach to model uncertainty. In Cases 1 and 5, the cooling capacity slightly exceeded the optimal value while the cost was below J^*. However, in these cases, the perturbations on the system were such that both the compressor and engine were more efficient than in the optimal case. Therefore, we expect to see $J < J^*$ despite $C_{achieved} \approx C^*_{achieved}$ in those two cases.

We see from Table 6 that for 10% variations in system parameters, the system operation remained within approximately 6% of the optimal operation setpoints. As a result, it can be said with some confidence that the approach of optimizing operational setpoints using the advocated exergy-based approach will be relatively robust to practical uncertainties in the system models.

Table 6
Average deviation from optimal operation.

Optimization variable	Units	Optimized value	Average deviation (%)
h_1	kJ/kg	257.1	0.78
h_2	kJ/kg	280.9	0.88
h_4	kJ/kg	104.4	5.91
P_1	kPa	288.0	2.98
$\dot{m}_r$	kg/hr	18.7	6.76
$\dot{m}_{AF}$	kg/hr	1.06	0.003

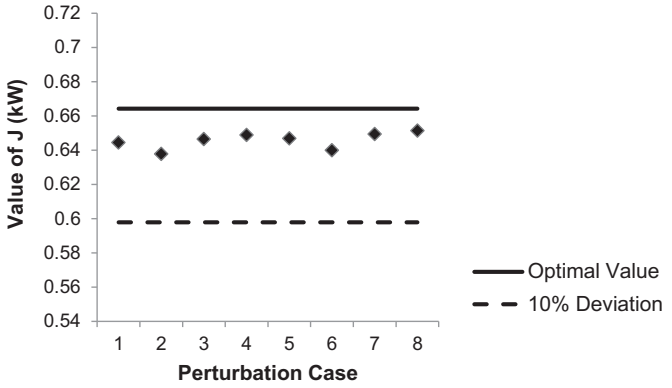

Fig. 8. Value of objective function, J, for each of 8 perturbation cases, relative to optimal value, J^*.

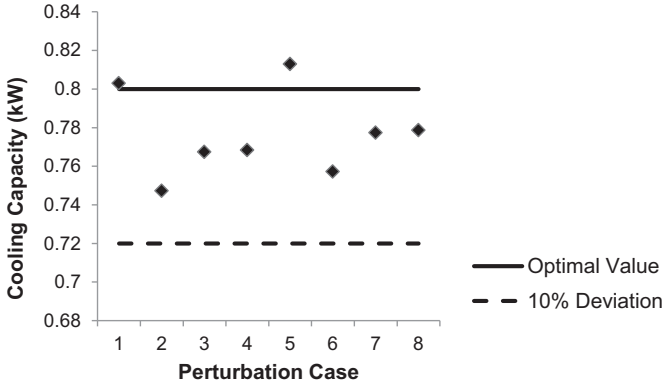

Fig. 9. Value of capacity achieved for each of 8 perturbation cases, relative to capacity achieved with optimal setpoints.

6. Conclusion

This paper introduced an exergy-based objective function for the steady-state optimization and control of integrated energy systems (IESs). The use of exergy destruction as the metric for minimization was motivated by the desire for an objective function which is generalizable to a wide class of IESs. More specifically, exergy destruction can be used to characterize irreversibilities across multiple energy domains (chemical, electrical, mechanical, thermal), making it very suitable for the types of energy subsystems which comprise IESs.

The optimization framework was demonstrated on an engine-driven VCC system. This system provided a suitable platform due to the fact that it spans multiple energy domains and is used commercially at multiple scales (smaller automotive systems to large building chillers). The objective function was derived entirely from first-principles. Nonlinear static model equations were used to define design constraints as well as to compute a set of feedforward control inputs for achieving the optimal operation setpoints.

It was shown that the primary advantage of the use of an exergy-based objective function is its physical significance and modularity. An alternative objective function, constructed using system-specific efficiency metrics, was very sensitive to weightings on each term given that the quantity being optimized was not physically relevant.

Finally, robustness of the estimated control inputs to modeling uncertainty and assumptions present in the static model equations

was successfully demonstrated. The achieved operation setpoints in eight different perturbation cases remained within approximately 6% of the optimal setpoint values.

In future work, the authors will explore the dynamic analog of this problem for real-time optimization in the presence of disturbances such as variation in ambient temperature as well as varying load profiles. Additionally, other types of subsystems spanning multiple energy domains will be added to determine the effectiveness and scalability of the proposed exergy-based approach.

Appendix A. Nonlinear parameter models

Appendix A.1. Fluid-mechanical VCC components

The models for valve flow coefficient (A.1) and compressor volumetric efficiency (A.2) for the particular IES considered in this paper were developed in [29] and are shown here for the reader's reference. While the coefficients of f_1 and f_2 are specific to a particular VCC system, the functional relationships described by f_1 and f_2 are typical of most electronic expansion valves (EEVs) and reciprocating compressors, respectively.

$$\hat{K}_v = f_1(a_v, P_1, P_2) = \left(-9.5984\times10^{-6}\right) + \left(2.0481\times10^{-6}\right)a_v + \left(5.4106\times10^{-9}\right)(P_2-P_1) + \left(-7.4909\times10^{-10}\right)a_v \times (P_2-P_1) + \left(-3.7775\times10^{-8}\right)a_v^2 \quad (A.1)$$

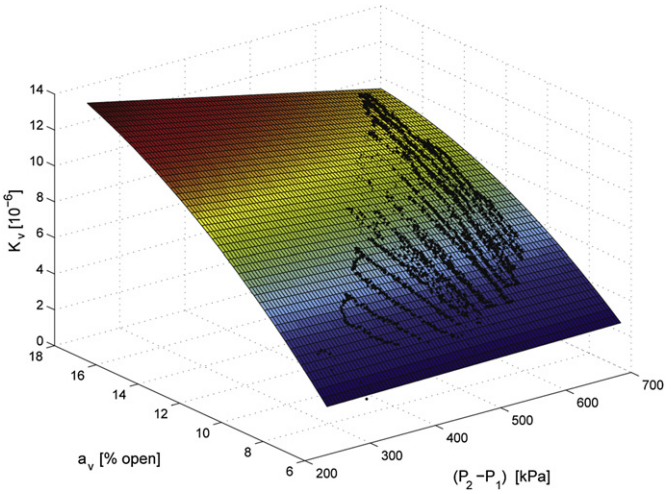

Fig. A.10. Flow coefficient map for an EEV [29]. Black points represent experimental data.

$$\hat{\eta}_{vol,k} = f_2(\omega_k, P_1, P_2) = (0.65127) + (0.00027681)\omega_k + (-0.031338)\frac{P_2}{P_1} + \left(3.0221\times10^{-5}\right)\omega_k\frac{P_2}{P_1} + \left(-1.1905\times10^{-7}\right)\omega_k^2 + (-0.0081256)\left(\frac{P_2}{P_1}\right)^2 \quad (A.2)$$

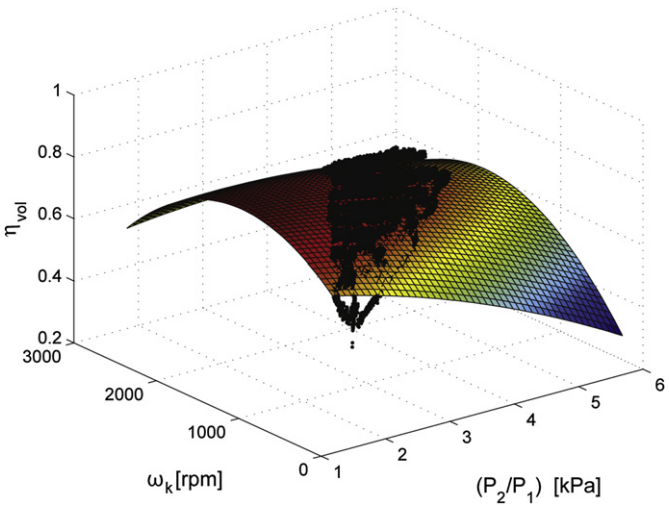

Fig. A.11. Volumetric efficiency map for a semi-hermetic reciprocating compressor [29]. Black points represent experimental data.

Appendix A.2. Thermal-fluidic VCC components

In general, the overall heat transfer coefficients of an evaporator and condenser, $(\widehat{UA})_L$ and $(\widehat{UA})_H$ respectively, can be computed using heat transfer correlations and a thermal resistance circuit (Fig. A.12) [20]. In order to estimate the UA-value for each heat exchanger, the following assumptions are made:

- The refrigerant in each heat exchanger is entirely a two-phase fluid,
- T_H and T_L are constant throughout the condenser and evaporator, respectively, and
- Fin heat transfer is one-dimensional.

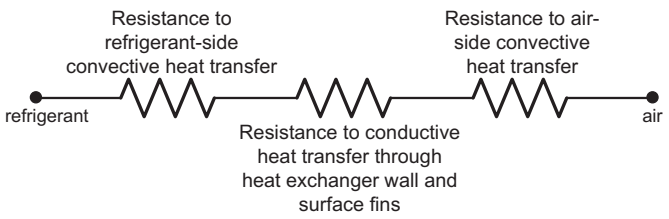

Fig. A.12. Thermal circuit used to compute overall heat transfer coefficient for condenser and evaporator.

$$\frac{1}{UA} = \frac{1}{\alpha_r A_i} + \frac{t}{kA_o(1-F_a)} + \frac{1}{\alpha_a A_o} \quad (A.3)$$

The correlations used to compute $\alpha_{a,e}$ and $\alpha_{a,c}$ for the specific evaporator and condenser considered in this paper are described in [29]. The correlations used to compute $\alpha_{r,e}$ and $\alpha_{r,c}$ are described in [30] and [31], respectively.

In order to estimate $(\widehat{UA})_{L,\max}$ and $(\widehat{UA})_{H,\max}$, it is assumed that the mass flow rates of air across the evaporator and condenser, respectively, are at their maximum.

Appendix A.3. SI–IC engine

The models for throttle plate angle Equation (43) and engine volumetric efficiency Equation (44) for the particular IES considered in this paper are described in [32] and shown here for the reader's reference:

$$\hat{\theta}_{\mathrm{tp}} = f_5(\dot{m}_{\mathrm{AF}}) = \frac{\cos^{-1}(1 - 1016.1\dot{m}_{\mathrm{AF}}) + 1.06^{\circ}}{1.14459} \tag{A.4}$$

$$\hat{\eta}_{\upsilon\mathrm{ol,eng}} = f_6(\omega_k) = \left(8.10 \times 10^{-4}\right)\omega_k + 0.352 \tag{A.5}$$

Appendix B. Convergence of optimization solution

The optimization problem consists of the nonlinear objective function, J, as well as multiple nonlinear constraints. Therefore, existence of a global optimum cannot be shown. Nevertheless, the optimality of the solution is demonstrated in Fig. B.13 where the identical optimization problem was gridded and solved over a span of different initial conditions.

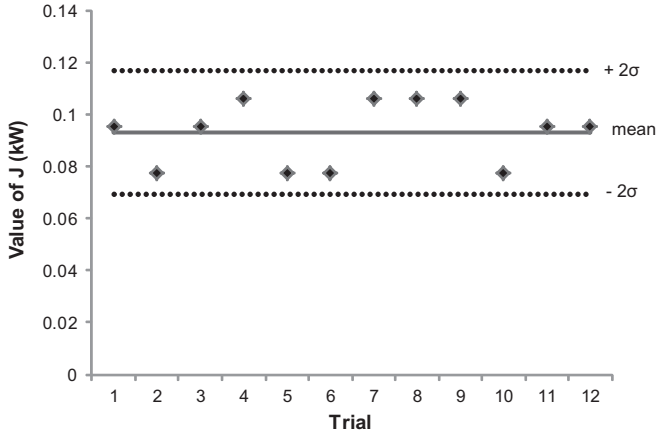

Fig. B.13. Demonstration of convergence of solution over constrained space for $C_{\mathrm{desired}} = 0.5$ kW, $\gamma = 0.05$, $\lambda = 0.1$, $T_L = 15^{\circ}C$, $T_H = 27^{\circ}C$, $r = 8$, $T_{1'} = T_H$, $P_{1'} = 101.3$ kPa.

For the domain of interest chosen, the solution converges to approximately the same minimum value, validating that the solution is a minimum in the constrained space. The mean value of the minimum cost across the 12 trials is 0.093 kW and the variance is 1.39×10^{-4} kW.

References

[1] D. Wu, R. Wang, Combined cooling, heating and power: a review, Progress in Energy and Combustion Science 32 (5–6) (2006) 459–495.
[2] Combined heat and power partnership (October 2011). URL http://epa.gov/chp/index.html.
[3] P. LeMar, Integrated Energy Systems (IES) for Buildings: A Market Assessment, Tech. Rep., Resource Dynamics Corporation, 2002.
[4] A. Abusoglu, M. Kanoglu, Exergoeconomic analysis and optimization of combined heat and power production: review, Renewable and Sustainable Energy Reviews 13 (9) (2009) 2295–2308.
[5] P. Ahmadi, I. Dincer, Exergoenvironmental analysis and optimization of a cogeneration plant system using multimodal genetic algorithm (mga), Energy 35 (12) (2010) 5161–5172.
[6] C. Casarosa, F. Donatini, A. Franco, Thermoeconomic optimization of heat recovery steam generators operating parameters for combined plants, Energy 29 (3) (2004) 389–414.
[7] A. Cihan, O. Hacıhafızoğlu, K. Kahveci, Energy–exergy analysis and modernization suggestions for a combined-cycle power plant, International Journal of Energy Research 30 (2) (2006) 115–126.
[8] O. Shaneb, P. Taylor, G. Coates, Optimal online operation of residential mu-CHP systems using linear programming, Energy and Buildings 44 (2012) 17–25.
[9] H. Cho, R. Luck, L. Chamra, Supervisory feed-forward control for real-time topping cycle chp operation, Journal of Energy Resources Technology 132 (2010) 012401.
[10] V. Tsourapas, A. Stefanopoulou, J. Sun, Dynamics, optimization and control of a fuel cell based combined heat power (chp) system for shipboard applications, in: American Control Conference, 2005. Proceedings of the 2005, IEEE, 2005, pp. 1993–1998.
[11] A. Petrov, A. Zaltash, S. Labinov, D. Rizy, R. Linkous, Dynamic performance of a 30-kw microturbine-based chp system, ASHRAE Transactions 111 (Pt 1) (2005) 111.
[12] X. Kong, R. Wang, X. Huang, Energy optimization model for a cchp system with available gas turbines, Applied Thermal Engineering 25 (2) (2005) 377–391.
[13] T. Reddy, I. Maor, Cost penalties of near optimal scheduling control of bchp systems: part II – modeling, optimization, and analysis results, ASHRAE Transactions 115 (1) (2009) 287–307.
[14] H. Cho, R. Luck, S. Eksioglu, L. Chamra, Cost-optimized real-time operation of chp systems, Energy and Buildings 41 (4) (2009) 445–451.
[15] E. Thorin, H. Brand, C. Weber, Long-term optimization of cogeneration systems in a competitive market environment, Applied Energy 81 (2) (2005) 152–169.
[16] S. Tassou, G. De-Lille, Y. Ge, Food transport refrigeration-approaches to reduce energy consumption and environmental impacts of road transport, Applied Thermal Engineering 29 (8–9) (2009) 1467–1477.
[17] M. Moran, H. Shapiro, Fundamentals of Engineering Thermodynamics, fifth ed. John Wiley and Sons Inc., New York, NY, 2003.
[18] N. Lior, G. Rudy, Second-law analysis of an ideal otto cycle, Energy Conversion and Management 28 (4) (1988) 327–334.
[19] A. Bejan, Advanced Engineering Thermodynamics, second ed. John Wiley and Sons, Inc., 1997.
[20] F. Incropera, D. De Witt, Fundamentals of Heat and Mass Transfer, John Wiley and Sons Inc., New York, NY, 1985.
[21] T. Coleman, M. Branch, A. Grace, Optimization Toolbox: For Use With Matlab (1999).
[22] W. Stoecker, J. Jones, Refrigeration and Air Conditioning, McGraw-Hill Book Company, 1983.
[23] B. Wu, C. Lin, Z. Filipi, H. Peng, D. Assanis, Optimal power management for a hydraulic hybrid delivery truck, Vehicle System Dynamics 42 (1–2) (2004) 23–40.
[24] Z. Filipi, L. Louca, B. Daran, C. Lin, U. Yildir, B. Wu, M. Kokkolaras, D. Assanis, H. Peng, P. Papalambros, et al., Combined optimisation of design and power management of the hydraulic hybrid propulsion system for the 6×6 medium truck, International Journal of Heavy Vehicle Systems 11 (3) (2004) 372–402.
[25] R. Johri, Z. Filipi, Low-cost pathway to ultra efficient city car: series hydraulic hybrid system with optimized supervisory control, SAE International Journal of Engines 2 (2) (2010) 505.
[26] M. Elliott, B. Rasmussen, in: A Model-Based Predictive Supervisory Controller for Multi-Evaporator HVAC Systems, American Control Conference, IEEE, 2009, pp. 3669–3674.
[27] B. Rasmussen, Dynamic Modeling and Advanced Control Of air conditioning and refrigeration systems, Ph.D. Thesis, University of Illinois at Urbana-Champaign (2005).
[28] B. Li, A. Alleyne, A dynamic model of a vapor compression cycle with shutdown and start-up operations, International Journal of Refrigeration 33 (3) (2010) 538–552.
[29] B. Eldredge, Improving the Accuracy and Scope of Control-Oriented Vapor Compression Cycle System Models, Master's Thesis, University of Illinois at Urbana-Champaign (2006).
[30] J. Wattelet, Heat Transfer Flow Regimes of Refrigerants in a Horizontal-tube Evaporator, Tech. Rep., Air Conditioning and Refrigeration Center, College of Engineering. University of Illinois at Urbana-Champaign, 1994.
[31] M. Dobson, J. Chato, Condensation in smooth horizontal tubes, Journal of Heat Transfer 120 (1998) 193.
[32] T. Deppen, Modeling, simulation, and control of a hybrid hydraulic powertrain, Master's Thesis, University of Illinois at Urbana-Champaign (2009).